Macromolecular Chemistry and Physics
www.mcp-journal.de

Crystalline Carbosilane-Based Block Copolymers: Synthesis by Anionic Polymerization and Morphology Evaluation in the Bulk State

*Hanna Hübner, Bart-Jan Niebuur, Oliver Janka, Lea Gemmer, Marcus Koch, Tobias Kraus, Guido Kickelbick, Bernd Stühn, and Markus Gallei**

Block copolymers (BCPs) in the bulk state are known to self-assemble into different morphologies depending on their polymer segment ratio. For polymers with amorphous and crystalline BCP segments, the crystallization process can be influenced significantly by the corresponding bulk morphology. Herein, the synthesis of the amorphous-crystalline BCP poly(dimethyl silacyclobutane)-*block*-poly(2vinyl pyridine), (PDMSB-*b*-P2VP), by living anionic polymerization is reported. Polymers with overall molar masses ranging from 17 400 g to 592 200 g mol^{-1} and PDMSB contents of 4.8–83.9 vol% are synthesized and characterized by size-exclusion chromatography and NMR spectroscopy. The bulk morphology of the obtained polymers is investigated by means of transmission electron microscopy and small angle X-ray scattering, revealing a plethora of self-assembled structures, providing confined and nonconfined conditions. Subsequently, the influence of the previously determined morphologies and their resulting confinement on the crystallinity and crystallization behavior of PDMSB is analyzed via differential scanning calorimetry and powder X-ray diffraction. Here, fractionated crystallization and supercooling effects are observable as well as different diffraction patterns of the PDMSB crystallites for confined and nonconfined domains.

1. Introduction

Crystallizable polymers usually exhibit an exothermal crystallization and an endothermal melting event at specific temperatures, named T_c and T_m, whereas the amorphous regions of the polymer are responsible for the glass transition temperature, T_g. These values are often considered as polymer-specific but can be affected by, e.g., additives, crosslinking, modulation of the thermal history of the polymer, or variation of the molecular weight. Here, the crystallization process is especially susceptible towards the presence of heterogeneities which usually determine the crystallization temperature, as there are almost always impurities or additives within the sample. These then act as crystallization nuclei leading to heterogeneous nucleation. In the absence of those crystallization nuclei, i.e., the neat substance without any impurities, homogeneous or surface-induced crystallization occurs, leading to a significantly reduced crystallization temperature due to the resulting higher free energy barrier. Also, confinement and the resulting surface effects can impact the crystallization temperature, which was shown and reviewed by several groups.[1–5] Especially when the size of the confined space is in the same order of magnitude as the crystallites, a drastic influence on the crystallization process and its orientation is expected.[1] This will become more and more important, especially in the field of nanotechnology and

H. Hübner, L. Gemmer, M. Gallei
Chair in Polymer Chemistry
Universität des Saarlandes
Campus Saarbrücken
66123 Saarbrücken, Germany
E-mail: markus.gallei@uni-saarland.de
B.-J. Niebuur, M. Koch, T. Kraus
INM – Leibniz Institute for New Materials
Campus D2 2, 66123 Saarbrücken, Germany
O. Janka, G. Kickelbick
Inorganic Solid-State Chemistry
Saarland University
Campus C4 1, 66123 Saarbrücken, Germany
T. Kraus
Colloid and Interface Chemistry
Saarland University
Campus D2 2, 66123 Saarbrücken, Germany
B. Stühn
Institute for Condensed Matter Physics
Technical University of Darmstadt
Hochschulstraße 8, 64289 Darmstadt, Germany
M. Gallei
Saarene, Saarland Center for Energy Materials and Sustainability
Campus C4 2, 66123 Saarbrücken, Germany
The ORCID identification number(s) for the author(s) of this article can be found under https://doi.org/10.1002/macp.202200178

DOI: 10.1002/macp.202200178

nanolithography, as the physical properties of confined crystallization deviates from crystallization in the bulk state, thus enabling different and potentially more complex structures compared to fully amorphous polymers.

Polysiloxanes are highly flexible and often crystalline materials. They find various applications in the field of coatings due to their mechanical properties and their high resistance against chemicals as well as environmental influences, as adhesion promoter or as sealing compound in form of silicone resins. Moreover, this class of polymers gained significant attention due to its possibility to perform as a preceramic material in order to generate, e.g., templated ceramic nanostructures by thermal treatment. Those hereby obtained ceramic materials, including nanocomposites and their preparation procedures, are reviewed by Orilall and Wiesner[6] and other authors.[7–13] In order to obtain oxygen-free ceramic materials, carbosilanes can be used, resulting in silicon-carbide ceramics.[14–17]

A polycarbosilane well known for its tendency to crystallize easily is poly(dimethyl silacyclobutane) PDMSB.[18–20] This becomes, for example, observable as the polymer precipitates due to occurring crystallization when synthesizing it by means of anionic ring opening polymerization (ROP) in tetrahydrofuran (THF) at low temperatures.[18,20,21] Anionic polymerization however, is an important synthesis tool for the control over the polymerization and the formation of block copolymers (BCPs). As BCPs possess the ability to self-assemble into microstructures, they have a huge potential for bottom-up strategies, especially in the case of PDMSB-based BCPs for nanolithographic purposes. Different BCPs with a PDMSB segment are known to literature such as poly(dimethyl silacyclobutane)-*b*-poly(methyl methacrylate) (PDMSB-*b*-PMMA),[22] poly(dimethyl silacyclobutane)-*b*-polystyrene (PDMSB-*b*-PS),[23–25] poly(dimethyl silacyclobutane)-*b*-poly(2-hydroxyethyl methacrylate) (PDMSB-*b*-PHEMA),[26] or as a BCP with different metallopolymers.[27] Also, triblock terpolymers, namely, poly(dimethyl silacyclobutane)-*b*-polystyrene-*b*-poly(2-vinyl pyridine) (PDMSB-*b*-PS-*b*-P2VP),[28–30] poly(dimethyl silacyclobutane)-*b*-polystyrene-*b*-poly(methyl methacrylate) (PDMSB-*b*-PS-*b*-PMMA),[31,32] and poly(dimethyl silacyclobutane)-*b*-polystyrene-*b*-polylactide (PDMSB-*b*-PS-*b*-PLA),[31,33,34] were described in the literature. Here, the main focus usually lies on the hydrophobicity of the carbosilane-based polymer and its potential application in lithography processes.[35]

To the best of our knowledge, only very little is known about the crystallization process of PDMSB-based BCPs. Kawahara et al. performed several differential scanning calorimetry (DSC) measurements as well as WAXS measurements on PDMSB, giving proof of the crystallinity of the analyzed material in the bulk state,[20] whereas Gallei et al. focused on the melting behavior of PDMSB on a curved surface leading to an overall diminished and even suppressed melting behavior.[18] Li et al. intensively studied the melting behavior of PDMSB homopolymers as they observed two endothermal signals while heating the sample during DSC measurements. Using isothermal crystallization at various temperatures and subsequent heating at different rates, they explained this complex melting behavior by postulating a recrystallization process, resulting in a deeper understanding of this multiple melting phenomenon.[19] But since the cooling rate was kept constant, still little is known about the crystallization process and its possibility to be influenced. Moreover, BCPs with an amorphous and a crystallizable polymer segment provide a more complex approach toward the crystallization behavior of PDMSB because of the influence of the amorphous polymer segment. Often, this influence is avoided by analyzing the crystallization of a polymer infiltrated in templated matrices (e.g., nanoporous anodic alumina oxide), as deposited droplets or dispersed in a liquid medium.[1,3,4,36–39] In the present study, the crystallization behavior of PDMSB in the form of a BCP with an amorphous second block segment P2VP is investigated. For this purpose, anionic ROP was used to synthesize BCPs with various block lengths to generate different microstructures which are known from amorphous BCPs, e.g., spheres and lamellae and characterize the influence of the self-assembled structures on the crystallization behavior of PDMSB. The polymers themselves were analyzed by size exclusion chromatography (SEC) and nuclear magnetic resonance (NMR) spectroscopy to determine the molecular weight and the composition of the polymer, followed by an analysis of the morphology by means of transmission electron microscopy (TEM) and small angle X-ray scattering (SAXS). Subsequently, the crystallization behavior of the PDMSB homopolymer and the corresponding BCPs was analyzed using differential scanning calorimetry (DSC) and powder X-ray diffraction (PXRD) taking the previously determined microstructures and the so potentially created confinement into account, in order to prove the susceptibility of the crystallization process towards confinement.

2. Results and Discussion

2.1. Synthesis and Characterization of Poly(1,1-dimethyl silacyclobutane)-*b*-poly(2-vinyl pyridine)

To obtain BCPs with an amorphous and a crystallizable polymer segment, PDMSB-*b*-P2VP was synthesized with different compositions via sequential anionic polymerization (**Scheme 1**). For this purpose, DMSB was polymerized in THF by initiation with *n*-butyllithium. After 1 h, an aliquot for SEC measurements of the formed PDMSB homopolymer was taken, diphenylethylene was added to the living polymer chains to prevent side reactions and 2VP was added subsequently to form the desired BCP altering the monomer ratio to obtain BCPs with different PDMSB/P2VP ratios and overall lengths. PDMSB is known to literature for its tendency to crystallize rapidly and is providing a hydrophobicity to the segment whereas P2VP is used as an amorphous, hydrophilic counterpart resulting in an amphiphilic BCP with an amorphous and a crystalline polymer segment.

The resulting polymers and taken aliquots were analyzed via SEC to determine the molecular weights and molar mass distribution. Here, the molecular weights of the PDMSB segments range from 11 300 to 24 900 g mol^{-1} according to the aliquots, whereas a clear shift toward higher molecular weights after the addition of P2VP proved the formation of a block copolymer. This is exemplarily shown in **Figure 1**a as the SEC trace of the PDMSB segment with a molecular weight of 16 500 g mol^{-1} is shifted to 40 100 g mol^{-1} after the addition of 2VP, suggesting an apparent molar mass growth of 23 600 g mol^{-1}. According to SEC measurements, PDMSB-*b*-P2VP block copolymers with a wide range of overall molecular weights from 17 400 up to 592 200 g mol^{-1} were obtained. However, it is noteworthy that the PDMSB homopolymer precipitates during the polymerization procedure,

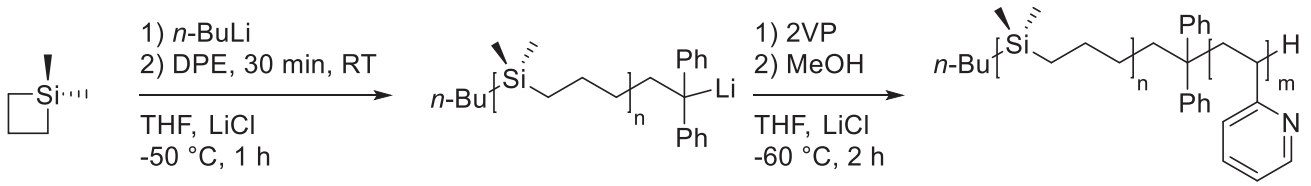

Scheme 1. Polymerization of 1,1-dimethyl silacyclobutane with *n*-butyllithium as the initiator in tetrahydrofuran at −50 °C with subsequent addition of 1,1-diphenylethylene to polymerize 2-vinyl pyridine at −60 °C.

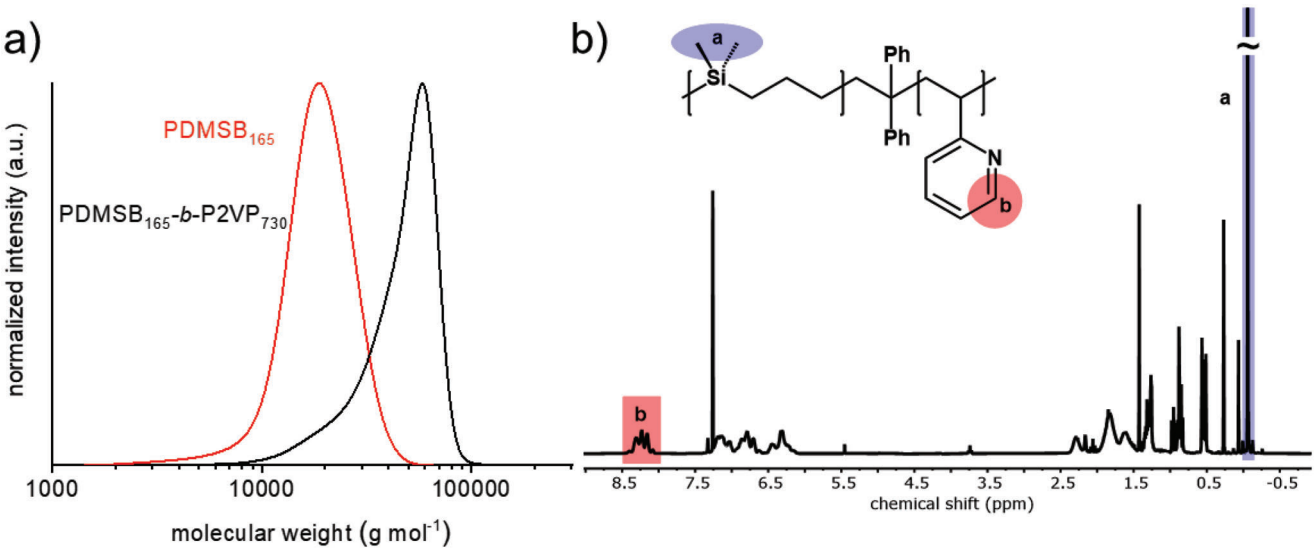

Figure 1. a) Molecular weight distribution of $PDMSB_{165}$-*b*-$P2VP_{730}$ and the corresponding PDMSB aliquot according to SEC measurements; b) ^{1}H NMR spectrum of $PDMSB_{165}$-*b*-$P2VP_{730}$ in $CDCl_3$.

giving rise to slightly increasing dispersity index values *Đ*, ranging from 1.09 to 1.54 (see Supporting Information). ^{1}H NMR spectroscopy analysis was performed to determine the composition and volume fraction of PDMSB when evaluating the integral of the signal at −0.061 ppm, which can be assigned to the dimethylsilane groups of PDMSB and at 8.16–8.31 ppm standing for P2VP (Figure 1b). The results indicate a broad spectrum of calculated volume fractions of PDMSB for the obtained BCPs ranging from 4.8 to 83.9 vol% and therefore potentially creating different microstructures upon self-assembly of the BCPs in the bulk state. Moreover, the molecular weight of the BCPs was calculated by taking the molecular weight of the PDMSB aliquot and the segment ratio of both polymer species into account. The degree of polymerization, calculated by the SEC data in the case of PDMSB and the data obtained from the respective ^{1}H NMR spectra for P2VP is indicated in the index, e.g., $PDMSB_{165}$-*b*-$P2VP_{730}$. All estimated and calculated molecular weights as well as the corresponding dispersities and the volume fractions of PDMSB are compiled in **Table 1**.

Table 1. Molecular weights of the synthesized homo- and block copolymers according to SEC and ^{1}H NMR measurements, the dispersity index values, and volume fractions of PDMSB.

	Polymer	M_n [a)] [kg mol^{-1}]	M_w [a)] [kg mol^{-1}]	$Đ$ [a)]	M_n [b)] [kg mol^{-1}]	vol% [c)] PDMSB
1	$PDMSB_{113}$-*b*-$P2VP_{2086}$	592.2	761.8	1.29	230.6	4.8%
2	$PDMSB_{153}$-*b*-$P2VP_{1479}$	539.1	773.2	1.43	170.8	8.9%
3	$PDMSB_{150}$-*b*-$P2VP_{842}$	43.7	54.1	1.24	103.4	14.3%
4	$PDMSB_{165}$-*b*-$P2VP_{730}$	40.1	48.6	1.21	93.2	17.5%
5	$PDMSB_{153}$-*b*-$P2VP_{639}$	232.2	253.4	1.09	82.5	18.3%
6	$PDMSB_{145}$-*b*-$P2VP_{541}$	138.6	170.2	1.23	71.4	20.1%
7	$PDMSB_{189}$-*b*-$P2VP_{514}$	94.3	145.6	1.54	72.9	25.7%
8	$PDMSB_{230}$-*b*-$P2VP_{286}$	39.7	47.9	1.21	53.0	43.1%
9	$PDMSB_{249}$-*b*-$P2VP_{214}$	39.4	60.7	1.54	47.3	52.3%
10	$PDMSB_{219}$-*b*-$P2VP_{135}$	37.6	45.1	1.20	36.0	60.5%
11	$PDMSB_{144}$-*b*-$P2VP_{82}$	27.2	33.1	1.21	23.0	62.3%
12	$PDMSB_{139}$-*b*-$P2VP_{25}$	17.4	21.7	1.25	16.5	83.9%
13	$PDMSB_{269}$	26.9	34.4	1.28	–	100.0%

[a)] Determined via SEC with THF as eluent at 1 mL min^{-1}, calibrated against polystyrene [b)] Determined via SEC of corresponding PDMSB aliquot and polymer ratio according to ^{1}H NMR [c)] Determined via ^{1}H NMR with densities of 1.102[17] and 1.14[40] for PDMSB and P2VP, respectively.

2.2. Analysis of Bulk Morphologies via TEM

The thermal properties comprising crystallization and glass transition temperature of the analyzed BCP can be significantly influenced by the self-assembled microstructures. Therefore, the

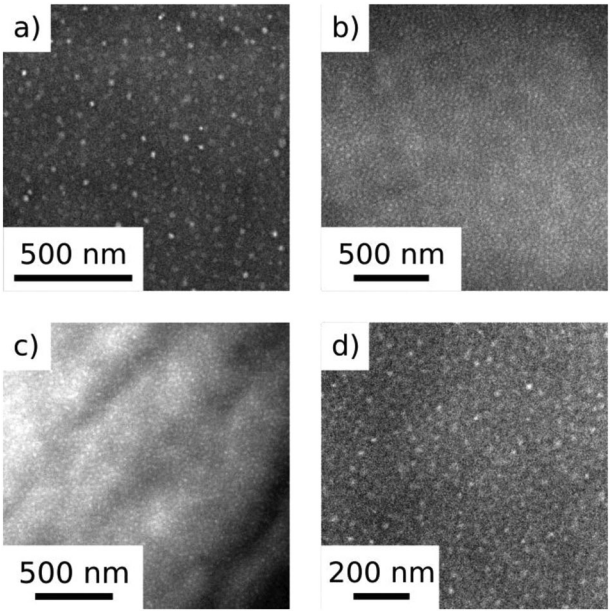

Figure 2. TEM images of spherical morphologies of a) $PDMSB_{153}$-*b*-$P2VP_{1479}$ (8.9 vol% PDMSB) with a domain size of 18 ± 3 nm, b) $PDMSB_{150}$-*b*-$P2VP_{842}$ (14.3 vol% PDMSB) with a domain size of 17 ± 3 nm, c) $PDMSB_{165}$-*b*-$P2VP_{730}$ (17.5 vol% PDMSB) with a domain size of 20 ± 3 nm, and d) $PDMSB_{145}$-*b*-$P2VP_{541}$ (20.1 vol% PDMSB) with a domain size of 16 ± 3 nm.

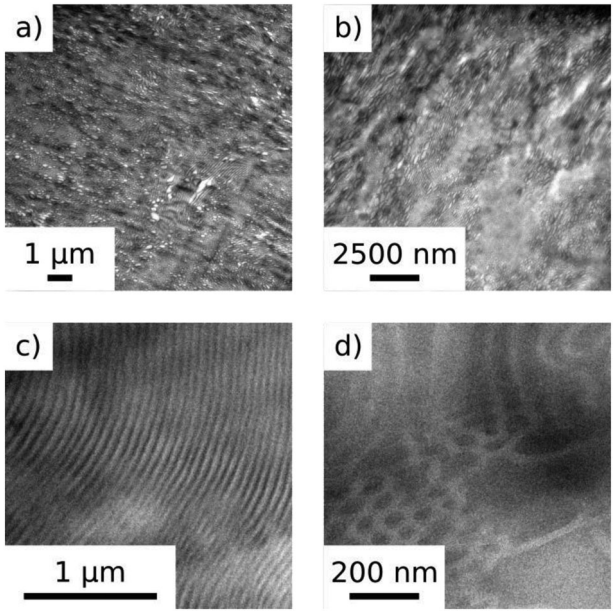

Figure 3. TEM images of a) mixed morphologies of $PDMSB_{230}$-*b*-$P2VP_{286}$ (43.1 vol% PDMSB), b) mixed morphologies of $PDMSB_{249}$-*b*-$P2VP_{214}$ (52.3 vol% PDMSB), c) lamellar morphologies of $PDMSB_{219}$-*b*-$P2VP_{135}$ (60.5 vol% PDMSB), and d) mixed morphologies with a PDMSB matrix of $PDMSB_{144}$-*b*-$P2VP_{82}$ (62.3 vol% PDMSB).

bulk morphologies of the prepared BCPs are first analyzed by means of TEM and SAXS, to gain a deeper understanding of the dependency of crystallinity and bulk morphology. To investigate the self-assembly behavior of the polymers, the microphase separation in the bulk state was analyzed via TEM. Here, the polymer films were solvent-casted from chloroform and thermally treated at 140 °C to improve the self-assembly and resulting microstructures. For polymers featuring a content of up to 25.7 vol% PDMSB, the images reveal that spheres were obtained as the bulk morphology (**Figure 2**), as expected from the volume ratio of both polymer species. The lighter areas in the TEM images representing the PDMSB segments with the lower volume fraction form spheres which are embedded in a P2VP matrix. The latter domains appear dark due to the aromatic system of the lateral bound pyridine moiety and the iodine staining, respectively. The diameters of the spheres determined via TEM are 18 ± 3 nm for the BCP with 8.9 vol% PDMSB, 17 ± 3 nm for 14.3 vol% PDMSB, 20 ± 3 nm for 17.5 vol% PDMSB, and 16 ± 3 nm for 20.1 vol%.

When increasing the amount of PDMSB, TEM images from the samples with 43.1 vol% PDMSB and 52.3 vol% PDMSB revealed morphologies that seem to be a mixture of different microstructures (**Figure 3**a,b). According to the volume fractions of the polymer segments, cylindrical, bicontinuous or lamellae structures would be expected, whereas the herein observed structures could be in an intermediate state between two structures and have not fully reached their thermodynamic equilibrium yet. This might happen due to insufficient solvent annealing or thermal treatment of the sample in order for the polymer to assemble into its thermodynamic stable morphology. Although both additional self-assembling strategies were used, still a plurality of morphologies is observable, which might be caused by the softness of the material. Therefore, the sample preparation, as well as the tendency of the PDMSB to crystallize rapidly, possibly resulting in break out crystallization, might alter the structures formed by self-assembly and microphase separation, leading to not clearly determinable structures.

For the sample with a volume fraction of 60.5% PDMSB lamellae structures were observed with a repeat distance of 30 ± 3 nm (Figure 3c). When increasing the PDMSB content further (62.3 vol% PDMSB), again mixed structures were obtained (Figure 3d) but in this case with the light PDMSB-rich domains as the predominant segment. Here, lamellae structures were visible as well as cylinders or a mixture of both. Finally, at a PDMSB content of 83.9 vol%, the sample could not be prepared by means of ultramicrotomy as the rising PDMSB content leads to an increased softness of the material.

2.3. Analysis of Bulk Morphologies via SAXS

To further investigate the self-assembled nanostructures of the BCPs, SAXS measurements were performed. **Figure 4** presents the small angle X-ray scattering of six samples. $PDMSB_{150}$-*b*-$P2VP_{842}$, featuring a PDMSB content of 14.3 vol%, shows a pronounced structure factor peak at ≈0.018 $Å^{-1}$, marking the presence of domains with a well-defined inter-distance. A secondary peak is visible at around 0.045 $Å^{-1}$, and at higher q-values, the scattered intensity decreases with q^{-4}, indicating that the boundaries between domains are sharp. The results from TEM (Figure 2) motivated us to fit the scattering using the form factor of spheres to describe the spherical domains formed by PDMSB multiplied with the structure factor of disordered hard sphere

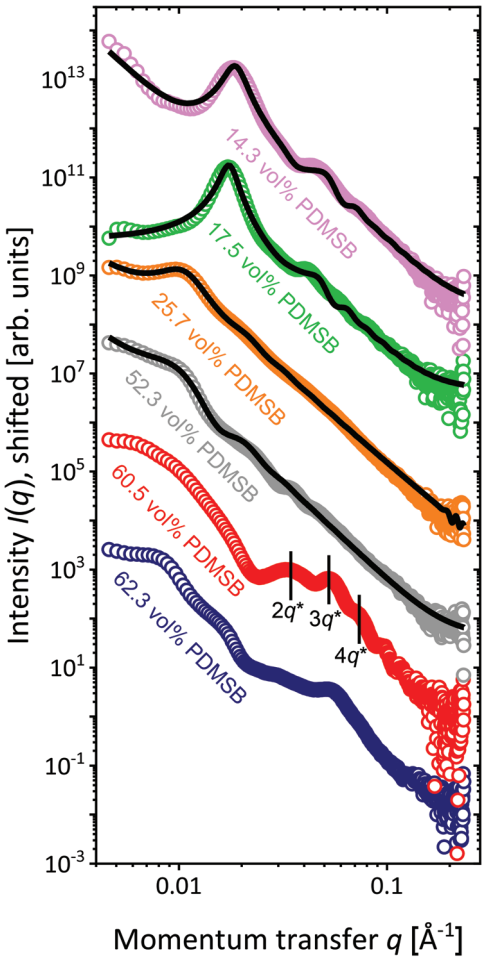

Figure 4. Scattering curves derived from SAXS measurements of selected BCP samples with PDMSB contents as given in the graph. The black lines are model fits using Equation (1).

packings [Equation (1)]. The fit matches the data in the entire measured q-range, showing that the dominating morphology is indeed composed of disordered spheres.

Increasing the PDMSB content up to 52.3 vol% in the case of $PDMSB_{249}$-*b*-$P2VP_{214}$, shifts the primary structure factor peak to smaller q values and reduces its magnitude, indicating that the distances between the sphere-centers increase and become more broadly distributed. The same fitting model for disordered spheres could be used to satisfactorily describe the data for all analyzed polymers containing up to 52.3 vol% PDMSB. For $PDMSB_{249}$-*b*-$P2VP_{214}$, with a PDMSB content of 52.3 vol%, the fit describes a morphology which was not clearly observable by means of TEM. Even though the fit describes the data reasonably well, the small deviations may suggest the presence of minor amounts of secondary structures, as suggested by TEM measurements (Figure 3a,b). The sphere radii and inter-domain distances for these samples resulting from the fits are given in **Table 2**.

The scattering curve of $PDMSB_{219}$-*b*-$P2VP_{135}$ with 60.5 vol% PDMSB depicts a high intensity at low q values, but a distinct primary Bragg reflection is not visible. This suggests the presence of several different morphologies, but the data are too limited for an

Table 2. Sphere radii and interdomain distances as determined by SAXS.

	Polymer	Average sphere radius R_{avg} [nm]	Interdomain distance [nm]
3	$PDMSB_{150}$-*b*-$P2VP_{842}$	11.9 ± 0.1	35.6 ± 0.2
4	$PDMSB_{165}$-*b*-$P2VP_{730}$	13.2 ± 0.1	39.2 ± 0.2
7	$PDMSB_{189}$-*b*-$P2VP_{514}$	9.2 ± 0.3	57.2 ± 0.2
9	$PDMSB_{249}$-*b*-$P2VP_{214}$	26.5 ± 0.2	55.6 ± 0.7

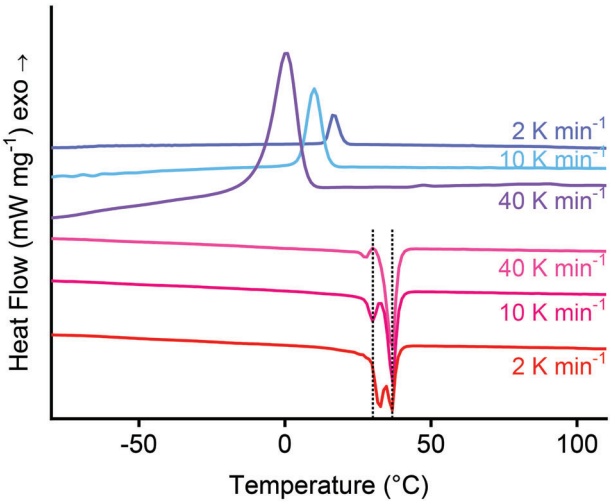

Figure 5. DSC thermograms of PDMSB homopolymer with various cooling rates (2, 10, and 40 K min^{-1}) and a constant heating rate of 10 K min^{-1}. Blue representing the cooling cycles, red the heating cycles. Dashed vertical lines are given to indicate the peak positions.

unambiguous reconstruction of morphology. Three pronounced secondary peaks are visible at q ratios of 2:3:4, which indicates that the dominating structure is composed of lamellae, with the primary Bragg reflection present at $q^* \cong 0.018$ $Å^{-1}$. This corresponds to a repeat distance of $D = 2\pi/q^* = 35$ nm, in reasonable agreement with the results from TEM (Figure 3c). The scattering curve of $PDMSB_{144}$-*b*-$P2VP_{82}$ containing 62.3 vol% PDMSB points to a mixed morphology, which may contain lamellae, indicated by a weak primary peak at $q^* \cong 0.008$ $Å^{-1}$ and secondary peaks at ≈0.016 $Å^{-1}$ ($2q^*$) and ≈0.032 $Å^{-1}$ ($4q^*$).

2.4. DSC Analysis of PDMSB Homo- and Block Copolymers

To finally evaluate the crystallization and melting behavior of PDMSB-*b*-P2VP, first, the corresponding behavior of the PDMSB homopolymer is analyzed by means of DSC. Li et al. varied the heating rates and applied isothermal treatment in their DSC measurements to determine their influence on the multiple melting phenomenon of PDMSB, but the significance of the cooling rate is yet unknown and an in-depth analysis of the crystallization behavior itself remains to be done. Therefore, in this study cooling rates of 2, 10, and 40 K min^{-1} were used whereas the heating rate was kept constant at 10 K min^{-1} (**Figure 5**). The hereby recorded crystallization signal shifts to lower temperatures with increasing cooling rates. For a cooling rate of 2 K min^{-1}, the crystallization signal was detected at 17 °C, for 10 K min^{-1} at

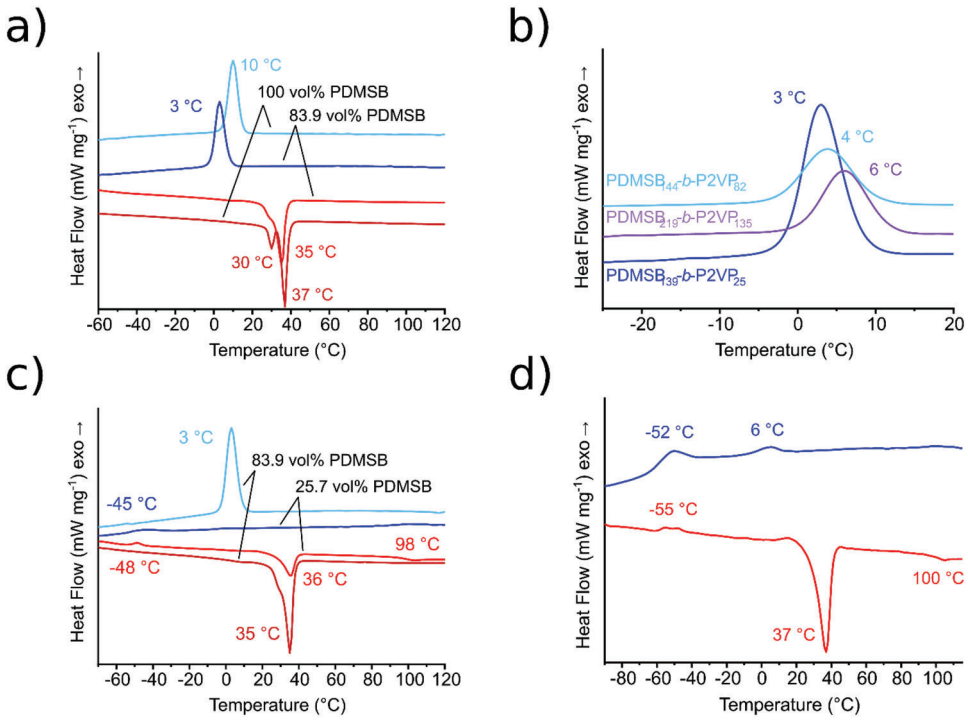

Figure 6. DSC thermograms of a) PDMSB homopolymer and PDMSB$_{139}$-*b*-P2VP$_{25}$ (83.9 vol% PDMSB), b) extract of cooling cycles of PDMSB$_{219}$-*b*-P2VP$_{135}$ (60.5 vol% PDMSB), PDMSB$_{144}$-*b*-P2VP$_{82}$ (62.3 vol% PDMSB), and PDMSB$_{139}$-*b*-P2VP$_{25}$ (83.9 vol% PDMSB), c) PDMSB$_{139}$-*b*-P2VP$_{25}$ (83.9 vol% PDMSB), and PDMSB$_{189}$-*b*-P2VP$_{514}$ (25.7 vol% PDMSB), and d) PDMSB$_{249}$-*b*-P2VP$_{214}$ (52.3 vol% PDMSB). Blue representing the cooling cycles, red the heating cycles.

10 °C and for 40 K min^{-1} at 1 °C. This can be explained by the fact that it takes time for the crystallization process to occur and proceed during the cooling process. Hence, crystallization takes place at lower temperatures and proceeds faster with increasing cooling rates. Interestingly, however, the overall crystallinity of the sample (determined via the crystallization enthalpy ΔH_C of the crystallization and both melting events) is independent of the applied cooling rate, which is a strong indicator for the rapid crystallization process of PDMSB. As the crystallization enthalpy of a fully crystalline PDMSB has not been determined yet, the absolute degree of crystallization cannot be calculated. Furthermore, no glass transition is observed, which, according to literature, is located at −55 °C.[20] This again indicates the likeliness of PDMSB to crystallize, which therefore creates only very little amorphous material, impeding a clear detection of the glass transition temperature. Moreover, the DSC measurements revealed that the first of the two melting events in the heating cycle is also influenced by the previously applied cooling rate. Upon decreasing the cooling rate, its intensity increases and it additionally shifts from 27 °C (40 K min^{-1}), via 30 °C (10 K min^{-1}) to 32 °C (2 K min^{-1}), moving closer to the final melting process, which occurs at about 37 °C and is independent of the previous cooling rate.

When analyzing the PDMSB-*b*-P2VP block copolymers with a high PDMSB content, as it is the case for, e.g., PDMSB$_{139}$-*b*-P2VP$_{25}$ with a PDMSB content of 83.9 vol%, similar results compared to the PDMSB homopolymer can be obtained, i.e., no glass transition, one crystallization and one melting event which is broadened due to the two melting events of PDMSB which are now combined to one signal with a peak at 35 °C and a significant shoulder at 30 °C (**Figure 6**a).

Whereas the melting temperature of PDMSB of the BCP agrees with the one of the PDMSB homopolymer, the crystallization temperature deviates significantly as it is shifted about 7 K toward lower temperatures. When analyzing several BCPs with a PDMSB content of 60.5, 62.3, and 83.9 vol%, still no T_g of P2VP is visible due to its low content but, the crystallization signal of PDMSB shifts to lower temperatures for lower molecular weights of P2VP. Figure 6b shows an overlay of the crystallization signals, revealing a shift from 6 °C, over 4 to 3 °C, whereas the PDMSB homopolymer reveals a crystallization temperature of 10 °C. This shift might be due to an incomplete phase separation of the two polymer segments, resulting in a partial dissolution of P2VP in the PDMSB phase which therefore, decreases the crystallization temperature.

In the case of BCPs with a PDMSB content below 50 vol%, as it is the case for PDMSB$_{189}$-*b*-P2VP$_{514}$ with a PDMSB content of 25.7 vol% (Figure 6c), the glass transition temperature of P2VP at 98 °C becomes visible as the P2VP content increases which agrees well with the literature.[41] On the other hand, the intensity of the melting signal of PDMSB decreases significantly as there is less PDMSB in the sample but the temperature of the signal stays comparable to the one of the homopolymer. The observed crystallization temperature however, shifts drastically by about 50 K to lower values, indicating a different crystallization behavior as in the PDMSB homopolymer or the previously analyzed block copolymers. According to the TEM and SAXS measurements, the morphology of the BCPs consists of PDMSB spheres imbedded

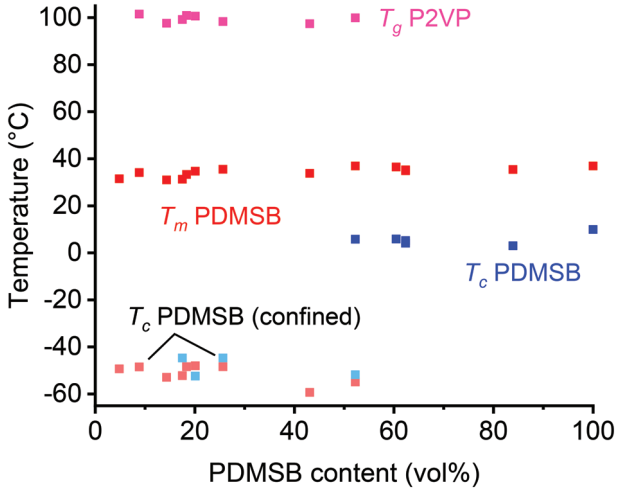

Figure 7. Compiled DSC results plotted against their PDMSB content. Blue data points are extracted from cooling cycles, red of heating cycles.

in an amorphous and solid P2VP matrix. Therefore, the crystallization of PDMSB is partially impeded as it occurs in confined spaces consisting of spheres with a diameter of about 15–20 nm embedded in a solid matrix, which significantly influences the crystallization process. Interestingly, the crystallization process does not seem to be completed after the crystallization event at −45 °C in the cooling cycle but continues in the following heating cycle at −48 °C. Here, it must be mentioned that those signals are in close proximity of the glass transition of PDMSB at −55 °C and therefore, the mobility of the polymer chains is significantly hampered, which may lead to a fractionated crystallization process.

Interestingly, for $PDMSB_{249}$-*b*-$P2VP_{214}$, with a PDMSB content of 52.3 vol% fractionated crystallization with exothermal events at 6 and −52 °C in the cooling cycle and at −55 °C in the heating cycle are observed (Figure 6d). Therefore, two different crystallization conditions must be present, which can be explained by the presence of a mixed morphology, as it was shown by TEM measurements previously. Therefore, the data suggest that there are confined PDMSB domains (crystallization signals at −52 °C in the cooling cycle and −55 °C in the heating cycle) as well as areas, where the crystallization of PDMSB is not confined and rather occurs in a manner similar to larger PDMSB domains or the homopolymer (crystallization signal at 6 °C). In addition, the glass transition of P2VP is observable at 100 °C.

When plotting the obtained melting, crystallization and glass transition temperatures derived from the DSC experiments of the BCPs against their PDMSB content (**Figure 7**), several trends become visible: Whereas the T_m of PDMSB remains more or less constant at about 35 °C, regardless of the ratio of both polymer segments, the T_g of P2VP at ≈100 °C becomes only visible below a PDMSB content of about 50 vol%. The crystallization temperature of PDMSB however, is the highest for the homopolymer (10 °C) and a little decreased in the case of the block copolymers with PDMSB as the major component. If the PDMSB content is lower than 50 vol%, the crystallization temperature drops drastically by about 55 K for all analyzed samples and no crystallization event at around 10 °C is visible anymore.

2.5. XRD Analysis of PDMSB Homo- and Block Copolymers

In order for the XRD samples to be able to self-assemble into their preferred morphology, the samples were heated to 150 °C and carefully cooled with liquid nitrogen to simulate a melting and cooling cycle comparable to the DSC experiments.

The XRD diffractograms of $PDMSB_{139}$-*b*-$P2VP_{25}$, providing a PDMSB content of 83.9 vol%, as well as $PDMSB_{219}$-*b*-$P2VP_{135}$ with a PDMSB content of 60.5 vol%, feature distinct Bragg reflections similar to those of the PDMSB homopolymer which are in good agreement to literature (**Figure 8**a),[20] revealing the same crystallization structure for the homopolymer and the analyzed BCPs. This resemblance of the XRD pattern of the BCPs toward the one of PDMSB homopolymer is expected due to the low P2VP content and agrees well with the previous results obtained via DSC (Figure 6a).

When the sample of $PDMSB_{144}$-*b*-$P2VP_{82}$ with a PDMSB content of 62.3 vol% is investigated in situ at 60 °C and therefore above the melting temperature of PDMSB, as determined in the DSC measurements, the previously observed reflections indicating crystalline PDMSB domains (Figure 8b, black) vanish and only an amorphous material is observable (Figure 8b, blue and red). When cooling the material back to 25°C, the reflections indicating crystallinity prior to the heating become visible again at the same position, proving the existence of the same crystalline material at 25 °C (Figure 8b, green). Although the previous DSC measurements suggest a crystallization temperature at about 10 °C for the according material, DSC experiments performed by Li et al. prove that previously heated material reveals a melting signal upon subsequent heating when applying an isothermal treatment at 298 K (25 °C).[19] Therefore, it can be assumed that an isothermal treatment below the melting temperature of PDMSB, i.e., at ≈37 °C, creates crystalline structures which are now detectable by means of XRD although not reaching the crystallization temperature determined via DSC, which is again a strong indicator for the tendency of PDMSB to crystallize rapidly.

For the measurements with $PDMSB_{165}$-*b*-$P2VP_{730}$, featuring a PDMSB content of 17.5 vol% and showing spheres according to TEM and SAXS analysis, the XRD experiments show reflections, indicating an at least partially crystalline material (Figure 8c). As expected, the intensity of the reflections is decreased and a significant amount of amorphous material is observed due to the lower PDMSB content and the increased amount of amorphous P2VP. Interestingly, the diffraction pattern is different from the ones observed in the diffractogram of the homopolymer and the block copolymers with PDMSB as the major component. The different positions of the reflections can be explained by the fact that crystallization now occurs under confinement due to the previously described microphase separation, leading to a different arrangement in the solid state. This again is in good agreement with the DSC measurements, which also indicate a different crystallization behavior when PDMSB crystallizes confined due to the microphase separation, resulting in different crystallization temperatures.

As the DSC of the BCP with 52.3 vol% PDMSB shows two crystallization temperatures, one indicating a crystallization of the material as it occurs in the homopolymer and one indicating confined crystallization, the material is analyzed subsequently by means of XRD. Figure 8d shows the corresponding results,

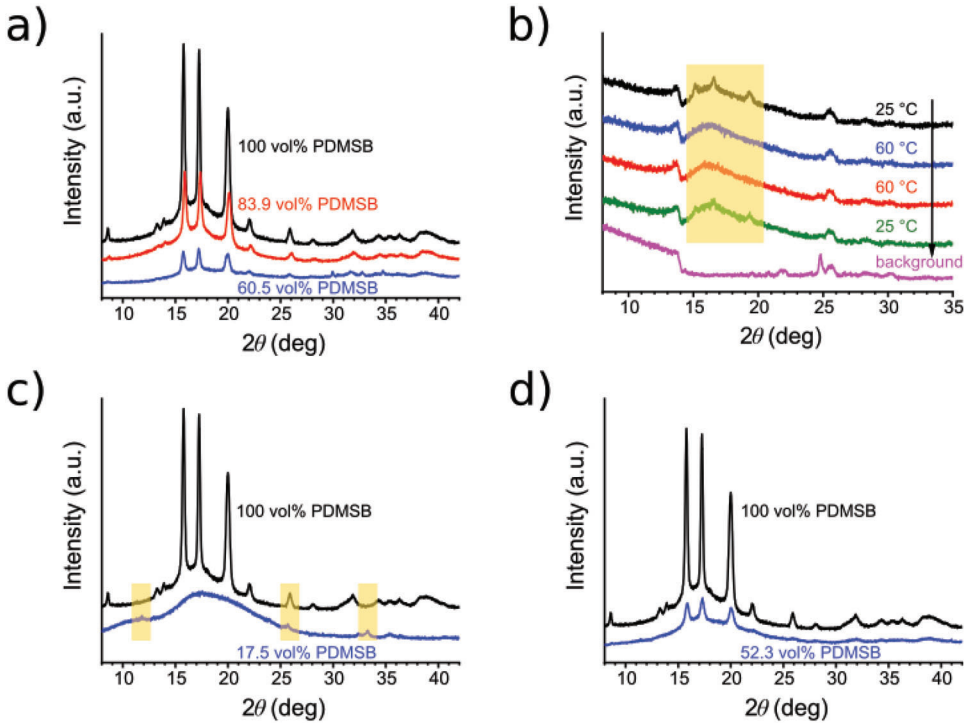

Figure 8. X-ray diffractograms of a) PDMSB homopolymer, $PDMSB_{139}$-*b*-$P2VP_{25}$ (83.9 vol% PDMSB), and $PDMSB_{219}$-*b*-$P2VP_{135}$ (60.5 vol% PDMSB), b) $PDMSB_{144}$-*b*-$P2VP_{82}$ (62.3 vol% PDMSB) at 25 °C, at 60 °C, and after cooling back to 25 °C, c) PDMSB homopolymer and $PDMSB_{165}$-*b*-$P2VP_{730}$ (17.5 vol% PDMSB), and d) PDMSB homopolymer and $PDMSB_{249}$-*b*-$P2VP_{214}$ (52.3 vol% PDMSB). Highlighted areas are given to point toward the pronounced differences for the reflexes and their positioning.

indicating only a crystallization behavior comparable to PDMSB homopolymer. This is surprising, since DSC and SAXS measurements suggest a crystallization pattern comparable to the sample with 17.5 vol% PDMSB due to the existence of spherical domains inducing a confined crystallization process. But as already seen in the sample with confined crystallization, the corresponding reflections turn out to be very small and might not be detectable since two different crystalline forms should be present in the sample with 52.3 vol% PDMSB according to DSC. Nevertheless, this sample remains remarkable since two different crystalline phases are visible within one polymer composition: SAXS proves the existence of spheres and therefore suggests a confined crystallization and TEM and XRD a non-confined crystallization, and DSC measurements were able to detect both crystallization forms.

3. Conclusion

In this study we synthesized PDMSB-*b*-P2VP, a block copolymer species comprised of an amorphous and a crystalline polymer segment, in various volume ratios and molecular weights. The polymers were characterized by means of SEC and ^{1}H NMR, followed by an analysis of their corresponding bulk morphology involving TEM and SAXS measurements, revealing spherical and lamellar domains as well as mixed phases. Subsequently performed DSC and XRD experiments revealed a clear dependency between the crystallization behavior of PDMSB and the previously determined bulk morphology: The spherical, PDMSB-rich domains are forced to crystallize under confinement due to the robust P2VP matrix and therefore result in a different diffraction pattern in the case of PXRD measurements and a drastically lower crystallization temperature in DSC experiments compared to a nonconfined crystallization process. The latter is comparable to the findings of PDMSB homopolymer characterizations. These results highlight the synthesis of novel amorphous-crystalline block copolymers in various compositions as well as the susceptibility of the crystallization process towards confinement effects. Tailoring the architecture of the polycarbosilane-based BCPs from a linear structure to a branched or grafted structure could further be applied to vary the confinement effect on the crystallizable domains as a change in the polymer architecture directly influences the self-assembled microstructures.[42–45]

4. Experimental Section

Reagents: All solvents and reagents were purchased from Fisher Scientific, ABCR, Sigma-Aldrich, and Alfa Aesar and used as received unless otherwise stated. Tetrahydrofuran (THF) was dried with a 1,1-diphenylhexyllithium solution and freshly distilled prior to use. LiCl was dispersed in dry THF and treated with *sec*-BuLi and stirred overnight. The solvent was removed under reduced pressure and the LiCl stored in a glovebox. DMSB and 2VP were dried overnight by stirring with CaH_2 and subsequently distilled. In the case of 2VP, the monomer was further treated with trioctylaluminum as a second drying reagent and again distilled under reduced pressure. The monomers were stored in a glovebox

at −20 °C. Methanol was dried over molecular sieve (3 Å), distilled under reduced pressure and stored in a glovebox.

Instrumentation: NMR spectra were recorded on a Bruker Avance II 400 spectrometer at 400 MHz and processed with MestReNova by Mestrelab Research. The chemical shifts are referenced relative to the deuterated solvent used. For SEC measurements an Agilent 1260 Infinity II setup with THF as the eluent at a flow rate of 1 mL min^{-1} was used. An SDV column set (1000, 5000, and 6000 Å) from polymer standard service (PSS, Mainz, Germany) and a PSS Security2 RI/UV detector were used. Calibration was carried out using PS standards (PSS Mainz, Germany).

TEM images were recorded on a JEOL JEM-2100 electron microscope at 200 kV acceleration voltage via a Gatan Orius SC1000 camera in bright field mode at a sample temperature of 19 °C. Software processing was carried out using Gatan Microscopy Suite.

SAXS measurements were performed on a Xeuss 2.0 instrument (Xenocs SAS, Grenoble, France). A collimated beam from the K_α-line of a copper X-ray source with a wavelength of $\lambda = 1.54$ Å was focused on the sample with a spot size of 0.64 mm^2. The samples with thicknesses of ≈1 mm were placed directly in the beam, i.e., without using a sample container, and were measured under vacuum conditions at room temperature. 2D scattering images with an acquisition time of 3600 s were recorded using a Pilatus 300K detector with pixel sizes of 0.172 × 0.172 mm^2 and a sample-to-detector distance of 2517 mm, calibrated using a silver behenate standard. In all cases, the scattering images showed no sign of anisotropic scattering. Therefore, they were azimuthally integrated to obtain $I(q)$. Here, q is defined as $q = 4\pi \times \sin(\theta/2)/\lambda$ with θ being the scattering angle. Scattering curves obtained for samples with PDMSB as the minor component were fitted using the function

$$I(q) = I_P(q) + S_{HS}(q)\, P_S(q) + I_{bkg}$$

Here, $I_P(q)$ denotes a generalized Porod law, accounting for large-scale structures.[46] $P_S(q)$ is a sphere form factor with a Gaussian size distribution, and yields the size of the spheres, R_S, and the width of the distribution, σ.[47] To account for the disordered arrangement of the spheres, $P_S(q)$ is multiplied with a hard-sphere structure factor, $S_{HS}(q)$.[48] It gives the hard sphere radius, R_{HS}, i.e., half the center-to-center distance between the spheres, and the hard-sphere volume fraction, η.

DSC was carried out with a DSC 214 F1 Polyma from Netzsch (Selb, Germany) with nitrogen as protective and purge gas in flow rates of 60 and 40 mL min^{-1}, respectively, in aluminum crucibles with a pierced lid. The sample was cooled to −100 °C and subsequently heated up to 150 °C to erase its thermal history. After cooling back to −100 °C, the temperature was held for 10 min and the sample was heated to 150 °C. The heating and cooling rate was 10 K min^{-1} unless stated otherwise. Obtained data were processed using the software Netzsch Proteus Thermal Analysis 8.0.1.

PXRD patterns of the samples were recorded at room temperature on a D8-A25-Advance diffractometer (Bruker, Karlsruhe, Germany) in Bragg-Brentano θ-θ geometry (goniometer radius 280 mm) with Cu $K\alpha$-radiation ($\lambda = 154.0596$ pm). A 12 µm Ni foil working as K_β filter and a variable divergence slit were mounted at the primary beam side. A LYNXEYE detector with 192 channels was used at the secondary beam side. Experiments were carried out in a 2θ range of 6°–55° with a step size of 0.013° and a total scan time of 2 h.

PXRD patterns at elevated temperatures were recorded on the same diffractometer using an XRK 900 (Anton Paar GmbH, Graz, Austria) reactor chamber. The samples were investigated in air at 25 and 60 °C with a heating rate of 5 K min^{-1}, respectively. After reaching 60 °C, the sample was kept at this temperature for 5 h, during which five diffraction patterns were recorded. Afterward, the sample was cooled to 25 °C by switching off the heating. The diffraction patterns were recorded between 5° and 50° 2θ with a step size of 0.013° and a total scan time of 1 h for each temperature.

Sequential Anionic Block Copolymerization of Dimethyl silacyclobutane and 2-Vinyl pyridine: Exemplary synthesis of poly(1,1-dimethyl silacyclobutane)-*block*-poly(2-vinyl pyridine) featuring a molar mass of 94.3 kDa ($PDMSB_{189}$-*b*-$P2VP_{514}$): In a glovebox, 14 mg (0.340 mmol) LiCl was added to 40 mL of dry THF, treated with *sec*-BuLi for purification followed by stirring at room temperature overnight. Afterward, 2188 µL (16.961 mmol) 1,1-dimethyl silacyclobutane was added and the reaction mixture was cooled to −50 °C. The reaction was initiated by a rapid addition of 21 µL (0.034 mmol, 1.6 M in hexane) *n*-BuLi via syringe. After 1 h, an aliquot was taken and quenched with degassed methanol. The active PDMSB chains were treated with 12 µL (0.068 mmol) 1,1-diphenylethylene followed by stirring for 30 min at room temperature. The mixture was then cooled to −60 °C and at −20 °C 307 µL (2.853 mmol) prechilled 2-vinyl pyridine was added. The reaction presumed at −60 °C for 2 h prior to the addition of traces of degassed methanol to terminate the polymerization. The polymer was precipitated in a tenfold excess of water, filtered and washed before drying in vacuo. The polymer was obtained as a white solid. The degree of polymerization (P_n) for PDMSB was determined according to the SEC measurement of the homopolymer aliquot whereas the P_n of P2VP was determined according to the previously determined molecular weight of the PDMSB and the polymer ratio determined via ^{1}H NMR. The P_n of each polymer will be indicated in the index after the respective polymer name ($PDMSB_{189}$-*b*-$P2VP_{514}$). SEC (vs PS): PDMSB: $M_n = 14\,400$ g mol^{-1}; $M_w = 16\,000$ g mol^{-1}; $Đ = 1.11$; PSMSB-*b*-P2VP: $M_n = 25\,600$ g mol^{-1}; $M_w = 32\,500$ g mol^{-1}; $Đ = 1.27$ (all SEC traces can be found in Figure 1 and the Supporting Information). ^{1}H NMR: (400 MHz, 300 K, $CDCl_3$, δ in ppm): 8.31–8.16 (m, N–CH pyridine), 7.20–6.31 (pyridine), 2.29–0.06 (alkyl), −0.06 (s, Si–$(CH_3)_2$).

Preparation of Block Copolymer Films: The BCP was dissolved in chloroform and the solvent was slowly evaporated at atmospheric pressure over several days. After thermal annealing at 140 °C, thin films of ≈40 nm were obtained using ultramicrotomy and placed on a copper grid. In some cases, additional staining of the P2VP domains with iodine vapor to provide a better material contrast for the TEM measurements was necessary.[49]

Supporting Information

Supporting Information is available from the Wiley Online Library or from the author.

Acknowledgements

Instrumentation and technical assistance for the PXRD measurements in this work were provided by the Service Center X-ray diffraction, with financial support from Saarland University and German Science Foundation (Project No. INST 256/349-1).

Open Access funding enabled and organized by Projekt DEAL.

Conflict of Interest

The authors declare no conflict of interest.

Data Availability Statement

The data that support the findings of this study are available from the corresponding author upon reasonable request.

Keywords

anionic polymerization, confinement, crystallization, microphase separation, morphology

Received: June 1, 2022
Revised: June 23, 2022
Published online: July 20, 2022

[1] G. Liu, A. J. Muller, D. Wang, *Acc. Chem. Res.* **2021**, *54*, 3028.
[2] R. M. Michell, A. J. Mueller, *Progr. Polym. Sci.* **2016**, *54*, 183.
[3] G. Shi, G. Liu, C. Su, H. Chen, Y.u Chen, Y. Su, A. J. Müller, D. Wang, *Macromolecules* **2017**, *50*, 9015.
[4] J. M. Carr, D. S. Langhe, M. T. Ponting, A. Hiltner, E. Baer, *J. Mater. Res.* **2012**, *27*, 1326.
[5] Y.-L. Loo, R. A. Register, A. J. Ryan, G. T. Dee, *Macromolecules* **2001**, *34*, 8968.
[6] M. C. Orilall, U. Wiesner, *Chem. Soc. Rev.* **2011**, *40*, 520.
[7] P. Innocenzi, L. Malfatti, *Chem. Soc. Rev.* **2013**, *42*, 4198.
[8] N. D. Petkovich, A. Stein, *Chem. Soc. Rev.* **2013**, *42*, 3721.
[9] I. E. Rauda, R. Buonsanti, L. C. Saldarriaga-Lopez, K. Benjauthrit, L. T. Schelhas, M. Stefik, V. Augustyn, J. Ko, B. Dunn, U. Wiesner, D. J. Milliron, S. H. Tolbert, *ACS Nano* **2012**, *6*, 6386.
[10] M. Rawolle, M. A. Niedermeier, G. Kaune, J. Perlich, P. Lellig, M. Memesa, Y.-J. Cheng, J. S. Gutmann, P. Müller-Buschbaum, *Chem. Soc. Rev.* **2012**, *41*, 5131.
[11] Y. Ren, Z. Ma, P. G. Bruce, *Chem. Soc. Rev.* **2012**, *41*, 4909.
[12] M.-S. She, T.-Y. Lo, H.-Y. Hsueh, R.-M. Ho, *NPG Asia Mater.* **2013**, *5*, e42.
[13] J. Zhou, G. R. Whittell, I. Manners, *Macromolecules* **2014**, *47*, 3529.
[14] E. Ionescu, H.-J. Kleebe, R. Riedel, *Chem. Soc. Rev.* **2012**, *41*, 5032.
[15] S. Kaur, M. Gallei, E. Ionescu, in *Organic-Inorganic Hybrid Nanomaterials* (Eds.: S. Kalia, Y. Haldorai), Springer International Publishing, Cham **2015**, pp. 143–185.
[16] G. Mera, M. Gallei, S. Bernard, E. Ionescu, *Nanomaterials* **2015**, *5*, 468.
[17] Q. D. Nghiem, D.-P. Kim, *Chem. Mater.* **2008**, *20*, 3735.
[18] M. Gallei, J. Li, J. Elbert, M. Mazurowski, A. Schönberger, C. Schmidt, B. Stühn, M. Rehahn, *Polymers* **2013**, *5*, 284.
[19] J. Li, B. Kuttich, M. Gallei, J. Elbert, M. Rehahn, B. Stühn, *Polymer* **2013**, *54*, 5703.
[20] S. Kawahara, A. Nagai, T. Kazama, A. Takano, Y. Isono, *Macromolecules* **2004**, *37*, 315.
[21] K. Matsumoto, H. Shimazu, M. Deguchi, H. Yamaoka, *J. Polym. Sci., Part A: Polym. Chem.* **1997**, *35*, 3207.
[22] K. Aissou, M. Mumtaz, G. Fleury, G. Portale, C. Navarro, E. Cloutet, C. Brochon, C. A. Ross, G. Hadziioannou, *Adv. Mater.* **2015**, *27*, 261.
[23] J. Garnier, J. Arias-Zapata, O. Marconot, S. Arnaud, S. Bohme, C. Girardot, D. Buttard, M. Zelsmann, *ACS Appl. Mater. Interfaces* **2016**, *8*, 9954.
[24] A. Legrain, G. Fleury, M. Mumtaz, C. Navarro, J. Arias-Zapata, X. Chevalier, I. Cayrefourcq, M. Zelsmann, *ACS Appl. Mater. Interfaces* **2017**, *9*, 43043.
[25] K. Aissou, M. Mumtaz, G. Portale, C. Brochon, E. Cloutet, G. Fleury, G. Hadziioannou, *Small* **2017**, *13*.
[26] K. Matsumoto, U. Mizuno, H. Matsuoka, H. Yamaoka, *Macromolecules* **2002**, *35*, 555.
[27] M. Gallei, S. Tockner, R. Klein, M. Rehahn, *Macromol. Rapid Commun.* **2010**, *31*, 889.
[28] K. Aissou, M. Mumtaz, A. Alvarez-Fernandez, J. Mercat, S. Antoine, G. Pécastaings, V. Ponsinet, C. Dobrzynski, G. Fleury, G. Hadziioannou, *Macromol. Rapid Commun.* **2018**, *39*, 1700754.
[29] K. Aissou, M. Mumtaz, H. Bouzit, G. Pécastaings, G. Portale, G. Fleury, G. Hadziioannou, *Macromolecules* **2019**, *52*, 4413.
[30] K. Aissou, M. Mumtaz, A. Alvarez-Fernandez, J. Mercat, S. Antoine, G. Pecastaings, V. Ponsinet, C. Dobrzynski, G. Fleury, G. Hadziioannou, *Macromol. Rapid Commun.* **2018**, *39*, e1700754.
[31] S. Lee, L.-C. Cheng, K. G. Yager, M. Mumtaz, K. Aissou, C. A. Ross, *Macromolecules* **2019**, *52*, 1853.
[32] K. Aissou, M. Mumtaz, P. Marcasuzaa, C. Brochon, E. Cloutet, G. Fleury, G. Hadziioannou, *Small* **2017**, *13*.
[33] S. Lee, A. Subramanian, N. Tiwale, K. Kisslinger, M. Mumtaz, L.-Y. Shi, K. Aissou, C.-Y. Nam, C. A. Ross, *Chem. Mater.* **2020**, *32*, 5309.
[34] K. Aissou, W. Kwon, M. Mumtaz, S. Antoine, M. Maret, G. Portale, G. Fleury, G. Hadziioannou, *ACS Nano* **2016**, *10*, 4055.
[35] L.-Y. Shi, A. Subramanian, L. Weng, S. Lee, K. Kisslinger, C.-Y. Nam, C. A. Ross, *Nanoscale* **2022**.
[36] A.-K. Grefe, B. Kuttich, L. Stühn, R. Stark, B. Stühn, *Soft Matter* **2019**, *15*, 3149.
[37] J. R. Burns, D. Turnbull, *J. Appl. Phys.* **1966**, *37*, 4021.
[38] R. Cormia, F. Price, D. Turnbull, *J. Chem. Phys.* **1962**, *37*, 1333.
[39] J. Koutsky, A. Walton, E. Baer, *J. Appl. Phys.* **1967**, *38*, 1832.
[40] W. Zha, C. D. Han, D. H. Lee, S. H. Han, J. K. Kim, J. H.o Kang, C. Park, *Macromolecules* **2007**, *40*, 2109.
[41] O. Urakawa, A. Yasue, *Polymers* **2019**, *11*, 1153.
[42] M. Appold, C. Rüttiger, B. Kuttich, B. Stühn, M. Gallei, *Macromol. Chem. Phys.* **2018**, *219*, 1700187.
[43] M. Olvera De La Cruz, I. C. Sanchez, *Macromolecules* **1986**, *19*, 2501.
[44] J. Park, S. Jang, J. K. Kim, *J. Polym. Sci., Part B: Polym. Phys.* **2015**, *53*, 1.
[45] J. Wang, M. Muller, *J. Phys. Chem. B* **2009**, *113*, 11384.
[46] G. Porod, *Kolloid-Zeitschrift* **1951**, *124*, 83.
[47] P. Linder, T. Zemb, *Delta Series*, Elsevier, Netherlands **2002**.
[48] J. K. Percus, G. J. Yevick, *Phys. Rev.* **1958**, *110*, 1.
[49] R. I. Stanković, R. W. Lenz, F. E. Karasz, *Eur. Polym. J.* **1990**, *26*, 359.

